

Article

Assessment of the Brittle–Ductile State of Major Injection and Confining Formations in the Alberta Basin

Mahendra Samaroo ^{1,*}, Rick Chalaturnyk ¹, Maurice Dusseault ², Judy F. Chow ³ and Hans Custers ³¹ Department of Civil and Environmental Engineering, University of Alberta, Edmonton, AB T6G 2R3, Canada² Department of Earth and Environmental Sciences, University of Waterloo, Waterloo, ON N2L 3G1, Canada³ Alberta Department of Energy, Edmonton, AB T5K 2G6, Canada

* Correspondence: samaroo@ualberta.ca

Abstract: Subsurface interaction between critically stressed seismogenic faults and anthropogenic fluid injection activities has caused several earthquakes of concern over the last decade. Proactive detection of the reverse and strike-slip faults inherent in the Alberta Basin is difficult, while identification of faults likely to become seismogenic is even more challenging. We present a conceptual framework to evaluate the seismogenic potential of undetected faults, within the stratigraphic sequence of interest, during the site-selection stage of fluid injection projects. This method uses the geomechanical properties of formations present at sites of interest and their current state of stress to evaluate whether hosted faults are likely to be brittle or ductile since the hazard posed by faults in brittle-state formations is generally significantly higher than that of faults in ductile-state formations. We used data from approximately 3100 multi-stress triaxial tests to calculate the Mogi brittle–ductile state line for 51 major injection and confining formations in the Alberta Basin and in situ stress and pore pressure data from approximately 1200 diagnostic fracture-injection tests to assess the last-known brittle–ductile state of each formation. Analysis of these data shows that the major injection formations assessed in the Alberta Basin were in a ductile state, with some confining (caprock) formations in a brittle state at the time of the stress measurements. Once current site-specific in situ stress data are available, our method enables site-specific assessment of the current brittle–ductile state of geologic formations within the zone of influence of large-volume fluid-injection projects and an evaluation of the associated potential for fault seismogenesis.

Keywords: induced seismicity; Alberta Basin; brittle–ductile state; critically stressed faults; high volume fluid injection; fluid-injection hazard; Mogi line; seismogenic carbonate formations; subsurface risk



Citation: Samaroo, M.; Chalaturnyk, R.; Dusseault, M.; Chow, J.F.; Custers, H. Assessment of the Brittle–Ductile State of Major Injection and Confining Formations in the Alberta Basin. *Energies* **2022**, *15*, 6877.

<https://doi.org/10.3390/en15196877>

Academic Editor: Kamel Hooman

Received: 25 August 2022

Accepted: 17 September 2022

Published: 20 September 2022

Publisher's Note: MDPI stays neutral with regard to jurisdictional claims in published maps and institutional affiliations.



Copyright: © 2022 by the authors. Licensee MDPI, Basel, Switzerland. This article is an open access article distributed under the terms and conditions of the Creative Commons Attribution (CC BY) license (<https://creativecommons.org/licenses/by/4.0/>).

1. Introduction

The presence of proximal geologic faults is a key hazard to many types of infrastructure projects, including major infrastructure projects located on the ground surface (e.g., water retention dams), in the subsurface (e.g., tunnels) and those that utilize the subsurface (e.g., subsurface fluid disposal, energy storage, geothermal projects). Critically stressed faults are of particular importance in infrastructure hazard assessments since small changes in subsurface stresses or pore pressure can trigger fault reactivation, resulting in ground displacement, earthquakes and out-of-zone migration of subsurface fluids.

However, critically stressed faults appear to be pervasive, even in seismically quiescent intraplate continental regions [1], and intraplate earthquakes can pose a non-negligible infrastructure hazard in such regions because of a paucity of seismic-resistant infrastructure in these historically aseismic locations [2]. Fault hazard assessment in such regions is challenging because of the lack of a fundamental scientific framework to understand seismogenesis, inadequate historical seismic records and the paradox between low strain accrual and sudden moment (energy) release of a stick–slip nature [3]. Fault hazard assessments conducted for fluid injection projects located in such regions usually focus on

the identification and avoidance of (known) faults or the curtailment of injected fluid volumes/pressures to limit induced seismicity occurrence in cases where (usually unknown) critically stressed faults have been intercepted or previously triggered [4].

Within the Alberta Basin, vertical and thrust faults are common [5,6], with brittle slip along these types of faults responsible for the major induced seismic events that have occurred to date [7,8]. In the Precambrian basement that underlies the Alberta Basin, extensive fracturing has been postulated to exist mostly at the sub-seismic scale, consisting of deeper brittle fault detachments and offsets overlain by the broad zones of folded and fractured sedimentary strata [9]. Detection of such types of faults (i.e., reverse and vertical to sub-vertical strike-slip faults) using conventional seismic methods is difficult because of low offsets and limited extent (i.e., below the seismic resolution limit) [10]. Most of the anthropogenic induced seismicity that has occurred to date in the USA and Canada has been caused by the inadvertent interception and triggering of such previously undetected/unmapped faults [11,12]. Fluid-injection-project fault hazard assessments that rely solely on identification and avoidance of known faults may therefore possess some inherent uncertainty regarding future induced seismicity generation potential. The availability of a screening method to assess fault seismicity-hazard potential at the site selection stage of fluid injection projects can therefore be a useful hazard mitigation tool.

Over the last decade, there has been increasing evidence that geological/geomechanical factors largely control induced seismicity hazard (i.e., felt induced seismicity), but the controlling factors have been unclear [13,14]. Pore pressure increase, for instance, has often been cited as a primary factor in induced seismicity generation [15]. However, recent research noted that only 10% of an extensive fault trace triggered in the Dallas–Fort Worth Basin was actually seismogenic (with seismicity occurring at relatively low levels of pore pressure increase), while approximately 90% of this fault trace was not seismogenic at all levels of pore pressure increase [16]. Additionally, in this case the pore pressure increase required to trigger faults proximal to disposal operations was much higher ($\Delta P = 0.34$ MPa) than that required to trigger distal faults ($\Delta P = 0.04$ MPa) [16]. While the importance of geomechanical features in fault seismogenesis has been recognized [17], there has been limited progress in identifying the main causal factors for fault seismogenicity. The increasing use of machine learning tools to analyze large datasets in this field has resulted in the creation of new lumped parameters (e.g., geologic susceptibility, integrated geological index, combined geomechanical index, etc. [18–20]), which have been proposed to account for the combined seismogenic influence of all geologic/geomechanical features. While such methods can be useful in hindcast analyses, there is an important need to identify specific geomechanical parameters that control fault seismogenic slip in order to enable site-specific data collection and induced seismicity risk assessment prior to the construction/operation of fluid-injection projects.

The upper 10–15 km of the continental crust hosts most of the crustal displacement and seismogenic faults, with the seismogenicity of this zone generally attributed to (brittle) fracture and/or stick–slip displacement in brittle rock and fault sequences [21–23]. The lower crust is considered ductile, with its rock sequences displaying plastic/viscous behavior, and faults in this zone are aseismic [21,22]. In faults that extend over the brittle–ductile zones, progressive displacement within the ductile zone can result in strain accumulation within the brittle zone and subsequent seismogenic shear across the entire fault system [24]. Earthquake seismic hazard is generally associated with stick–slip displacement within brittle faults, while slip/displacement of ductile faults is generally aseismic and poses negligible seismic hazard [25]. Relatively small changes in confining stress can cause sedimentary rock sequences to transition from a (brittle) seismogenic state (i.e., unstable, stick–slip) to a (ductile) aseismic state and vice versa, with this mechanism postulated to primarily account for earthquake activity in deep sedimentary sequences [26].

While mature fault zones are generally weak, fault and host-rock deformation mechanisms and rheology can vary considerably over short distances (i.e., inside or outside the localized deformation zone) and timescales (earthquake recurrence cycles), since these de-

pend on thermodynamic conditions, rock properties and mechanical state [27]. Variations in material composition along a fault can also determine if fault displacement is seismogenic (i.e., if fault movement is seismic or aseismic) even within fault sections considered brittle [27–29]. Ductile fault host rock behavior is possible at depths of less than 5 km under conditions of high differential stress [30], pore pressure [30], confining pressure [31], porosity [32] and clay content [33]. Ductile rock sequences are likely to host ductile faults since the fault is expected to display the rheological behavior of the host material, and consequently, slip along such fault is expected to be aseismic. Conversely, brittle rock sequences are likely to host brittle faults, with slip along such faults anticipated to be brittle.

In some cases (physical/chemical), alteration of the rocks in the fault zone may alter the behavior of the fault shear-zone, either increasing [34] or decreasing [35] its brittleness relative to the host rock formation. For instance, higher dolomite mineral content in a carbonate formation increases formation and shear zone brittleness [36], with previous research linking the occurrence of some fluid-injection-induced seismic events to specific dolomitized regions of deep (high confining stress and pore pressure) Devonian platform carbonates present throughout the Alberta Basin [37]. While these extensive, highly fractured (low clay content, low-porosity) carbonate formations are important hydrocarbon and fluid disposal reservoirs [38], under certain conditions, these deep (often brittle) carbonates can be nucleation sites for significant earthquakes [39]. Therefore, the ability to assess (at the site screening stage) the seismogenic potential of carbonate formations within the zone of influence of large-scale fluid injection projects in this basin could help mitigate future fluid-injection project seismic risk.

Prior work indicated that the location of fluid-injection-induced earthquakes in Alberta is primarily influenced by geologic factors [18,40]. This research assesses the relative brittleness and the brittle–ductile limits of most of the major injection formations and confining sequences (caprock and underburden) in the Alberta Basin, using the Mogi relationship and rock mechanical properties obtained from multi-stress triaxial testing. We subsequently present and demonstrate the use of a conceptual framework to evaluate the in situ brittle–ductile state of each formation with reference to its Mogi line, using available in situ stress and formation pore pressure measurements. Our results indicate that, at the time of the in situ stress and pore pressure measurements, the major injection formations assessed were in the ductile state, with some caprock formations in the brittle state. However, the in situ stress data available for most of the deep (carbonate-rich) formations in seismogenic regions are likely outdated since they predate recent localized high-volume fluid injection trends occurring in this basin [4], and changes in fluid injection/extraction are known to alter the stress condition in rocks [41]. Our analysis indicates that one such formation (the Belloy) that was historically depleted and close to its brittle state has experienced notable induced seismic events triggered by recent industrial-scale fluid disposal activities. Our conceptual framework could be useful, in conjunction with contemporaneous site-specific (in situ stress and pore pressure) data, to evaluate the seismogenic potential of future industrial-scale fluid injection project sites in carbonate-rich stratigraphic sequences in this basin.

2. Materials and Methods

The extensive history of oil and gas development in the Alberta Basin, combined with the province's policies on data collection and open data access, resulted in the creation of one of the world's most comprehensive collections of publicly available geoscience data. This includes operational data such as fluid production and injection volumes, formation pressures and well logs, as well as geological, geomechanical, chemical and other types of laboratory analyses. The Alberta Energy Regulator maintains lists of data types and availability on its website (<https://www.aer.ca/providing-information/data-and-reports/activity-and-data> (last accessed 16 September 2022)), with the data catalog for tests conducted on almost all core samples collected in the Alberta Basin located at <https://static.aer.ca/prd/documents/sts/GOS-REPS.xlsb> (last accessed 16 September

2022). Submission of all laboratory core-test data for all cores collected is a component of regulatory requirements in the province and, therefore, mandatory for operators in Alberta. However, there is currently no standard submission format for the different types of laboratory core tests conducted, and consequently, significant variability exists in the type and format of data provided. A significant amount of data curation and interpretation was required to compile the database used for regional analyses across the basin.

2.1. Identification of Major Injection Formations in the Alberta Basin

Injection fluid operational data were used to identify all wells in Alberta that have injected any volume of fluid into the subsurface over the period from January 1960–December 2021, along with the type and volume (at surface conditions) of fluid injected and the injection stratigraphic zone (i.e., target receiving formation). This analysis showed that approximately 33,000 wells injected approximately 25 cubic kilometers (km^3) of water, 692 km^3 of gas and 3.35 km^3 of cold-water-equivalent steam (all measured at surface conditions) into the subsurface in Alberta during this period. We then grouped these wells according to the lithology and geologic age (era and period) of the injection formation and calculated the proportion of the total basin-wide volume of each type of fluid injected into each lithological group in each geologic age. We present the results of this analysis in Section 3.

2.2. Determination of the Mogi Brittle–Ductile State Limits for Major Formations and Confining Sequences in the Alberta Basin

The AER's core and drill cutting material sampling database (as of December 2021) contained approximately 600 individual reports (in secure pdf format) that included laboratory core triaxial tests. However, only a third of these reports contained the results of multistage triaxial tests; the remainder consisted of single-stage triaxial tests. Additionally, many reports contained the results of multiple core triaxial tests conducted on samples from different stratigraphic horizons within the same well. Figure 1a below shows the triaxial core-sample well locations, the type of triaxial test data available and the location density of fluid injection wells across the basin. Figure 1b shows the relative locations of known significant fluid-injection-induced seismic events that have occurred in the Alberta Basin to date.

The multistage triaxial data were contained in individual reports, each corresponding to a single well (or an individual sample in some cases). Manual data extraction, processing and data entry were required to aggregate the data and enable further analysis. Additionally, while each core-test laboratory report contained the unique well identifier (UWI) for each source well and the core sampling intervals, in some cases, the originating formation details were missing. This necessitated a geological review of the corresponding well logs for approximately 40% of the multistage triaxial core sample wells to identify the geologic formations and lithologies corresponding to each of the core samples tested. Additionally, in approximately 30% of the laboratory reports, only raw triaxial data were available; in such cases, processing and interpretation of the data were required to obtain the required formation geomechanical parameters. By using these data, we compiled approximately 3000 multistage triaxial tests corresponding to most of the major lithological sequences in the Alberta Basin (Table 1).

Table 1 shows that approximately 91% of the multistage triaxial tests available were conducted in low permeability (calcareous shale, calcareous sandstone or shaly limestone) lithologies, generally with the objective of measuring geomechanical properties important for hydraulic fracturing design (for tight oil exploitation) or caprock characterization (for thermal oil exploitation) in cases of shallow shale formations. The other major category of multistage triaxial tests data available was collected for the purposes of subsurface salt cavern design, and the wells drilled for these purposes provided geomechanical data for multiple adjacent formations in each area of interest. This information was then used to build an Excel database containing the core-sample originating formation, core depth

and laboratory-measured parameters for each sample, including confining stress (σ_3), failure stress (σ_1), unconfined compressive strength (C_0), Young's modulus (E), Poisson's ratio (ν), porosity (n), cohesion (c), angle of internal friction (φ) and Biot's coefficient (α). All the reports examined stated that the laboratory triaxial tests were conducted under drained conditions.

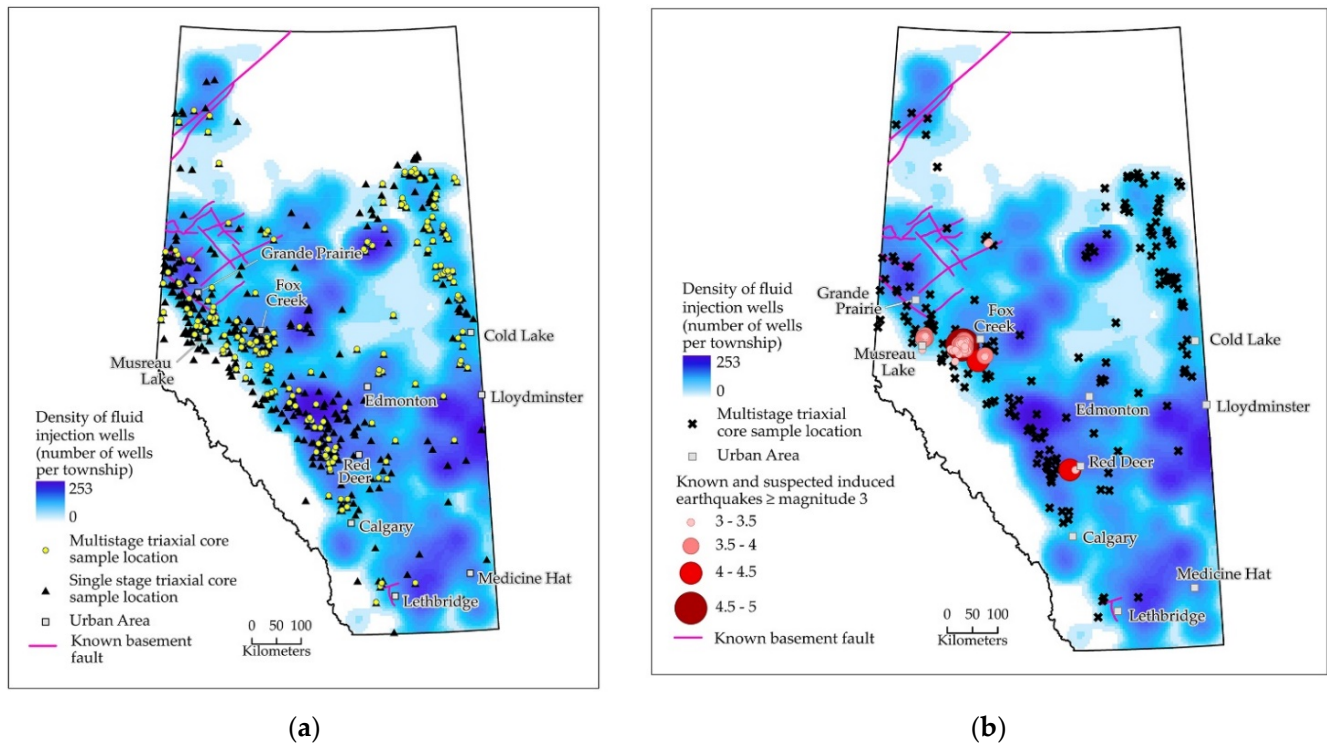


Figure 1. (a) Location of (approximately 600) triaxial core samples (triangles), (approximately 200) multistage triaxial samples (circles) and density of approximately 33,000 wells reporting some fluid injection over the period 1960–2021. (b) Location of known and suspected significant fluid-injection-induced earthquakes that have occurred in the Alberta Basin to date. Known regional basement faults are indicated by red lines.

Table 1. Summary of the number of multistage triaxial tests used in this analysis and the source lithologies.

Geologic Era	Major Lithology	No. of Wells	No. of Multistage Triaxial Core Tests	Proportion of Analyses (%)
Mesozoic	Shale	56	490	16
Mesozoic	Sandstone	58	716	24
Mesozoic	Limestone	17	147	5
Paleozoic	Calcareous shale	67	1105	37
Paleozoic	Calcareous sandstone	7	67	2
Paleozoic	Limestone	42	413	14
Paleozoic	Anhydrite	13	77	3
Total		260 ¹	3015	

¹ In some cases multiple core samples were collected from the same well.

This database was then used to determine confining stress at the brittle–ductile transition (σ_3^*) and to calculate the empirical Mogi ductility parameter (d) for each formation in accordance with the methods provided by Walton, 2021 [42]. First, the confining stress at the brittle–ductile transition (σ_3^*) for each formation was determined by reviewing the stress–strain curves of each of the (approximately 3000 triaxial tests), using the method shown in Figure 2 below.

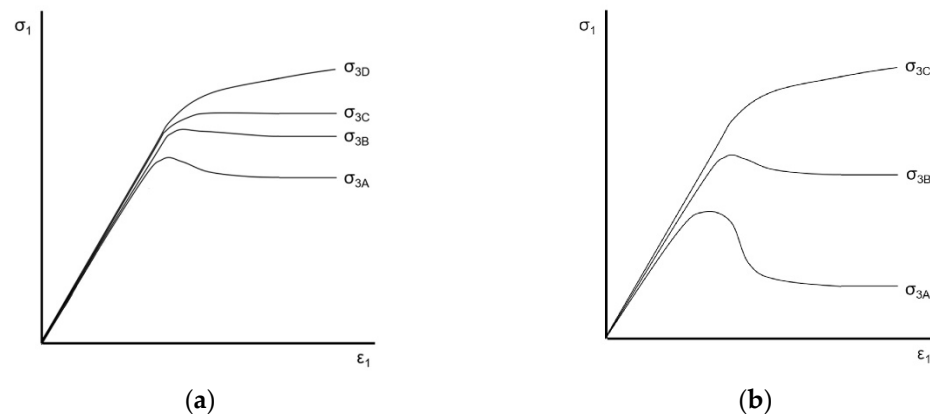


Figure 2. Illustration showing how multistage triaxial stress–strain curves were used to determine the principal and confining stresses at the brittle–ductile transition (σ_3^*) for each formation (a) Multistage triaxial test result with good confining stress resolution; $\sigma_3^* = \sigma_{3C}$ (b) Multistage triaxial test result with poor confining stress resolution; $\sigma_{3B} < \sigma_3^* < \sigma_{3C}$. Modified from Walton, 2021, and used with permission.

The empirical Mogi ductility parameter (d) was then calculated using Equation (1):

$$d = (\sigma_1 - \sigma_3^*) / \sigma_3^*, \quad (1)$$

where σ_1 and σ_3^* are the principal and confining stresses, respectively, at the Mogi brittle–ductile transition limit.

While the empirical Mogi ductility parameter (d) provides a useful index for the relative brittleness of rocks, it is highly dependent on the strength of the rock [42]. Walton (2021) notes that it is necessary to normalize the ductility parameter by the unconfined compressive strength (C_o) of the rock to obtain a normalized ductility parameter (termed d^*) that is independent of the unconfined compressive strength of the rock. This modified ductility parameter includes both rock strength (i.e., C_o) and material parameters (d), is directly comparable to existing brittleness indices, and can be used to quantitatively compare the brittleness of different rock formations [42]. Walton (2021) also notes that the d^* evaluated based on the stress–strain curves in the ductile regime can be considered an inherent material property, directly comparable to the modified Hoek–Brown material constant (m), which is extensively used in the geotechnical/geomechanical fields [43].

By using our Excel database, we then calculated the average unconfined compressive strength of each rock formation and then calculated the modified ductility parameter (d^*) in accordance with Equation (2):

$$d^* = d / C_o, \quad (2)$$

where C_o is the average measured unconfined compressive strength of the corresponding rock formation (in MPa). We present the results of this analysis in Section 3.

2.3. Determination of the Brittle–Ductile State Parameter and Brittle–Ductile Stress Index for Each Major Injection Formation and Confining Sequence in the Alberta Basin

The standard Mogi ductility parameter (d) provides the confining stress limit at which the transition from brittle fracture to ductile flow can be expected to occur [44] in each of the 51 formations assessed in the Alberta Basin, while the modified d^* provides a quantitative measure of the relative brittleness of the formations assessed. However, in

order to determine whether a formation is likely to be in a brittle or ductile state at its initial in situ stress regime, it is necessary to evaluate the relationship between its initial in situ stress state and its Mogi state limit. Such an evaluation also can provide an indication of whether sections of geologic faults contained within such formations are likely to be in a brittle or ductile state since hosted faults are likely to reflect the Mogi state of the host formation (especially in the low-porosity, low-clay content formations such as the deep carbonates of the Alberta Basin). Therefore, an evaluation of the brittle/ductile state of a formation can help provide an indication of the probability of the existence of brittle faults within rock sequences and consequently an indication of potential seismic hazards.

We devised a method based on the principles of the critical state concept applied to rock [45] to evaluate the in situ stress state of a formation relative to its Mogi line (considered the critical state line for rocks in this case). We used this concept, shown in Figure 3 below, to derive two associated parameters, called the Brittle–Ductile State Parameter (χ) and the Brittle–Ductile Stress Index (I_{BD}), shown in Equations (3) to (6). These two parameters can be used to assess whether a formation, at its current in situ stress state, may be in the brittle or ductile regime in relation to its Mogi state limit and, by extension, whether it is likely to host brittle (potentially seismogenic) faults.

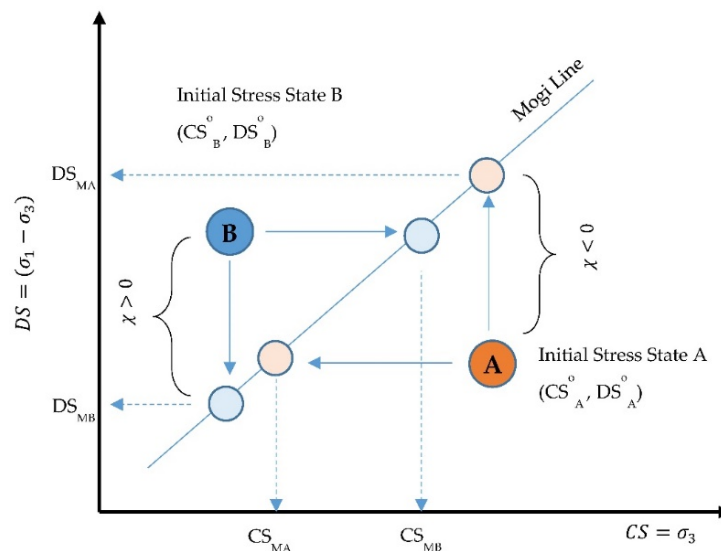


Figure 3. Concept and method used to derive the Brittle–Ductile State Parameter (χ) and the Brittle–Ductile Stress Index (I_{BD}). DS = Deviator stress; CS = Confining Stress; A and B are formations at initial confining and deviator stress states (CS^0 , DS^0).

In Figure 3, Formation A at an initial confining stress CS_A^0 and deviator stress DS_A^0 is in the ductile regime with respect to its Mogi line. Since the Mogi line relationship (i.e., the ductility parameter d , which is the gradient of the Mogi line in Figure 3) is known, Equation (1) above can be used to calculate the equivalent confining (CS_{MA}) and deviator (DS_{MA}) stresses at the Mogi line for the initial stress state (CS_A^0 , DS_A^0) of Formation A in accordance with the following relationships:

$$DS_{MA} = (\sigma_1 - \sigma_3)_{MA} = d^* \sigma_3^0_A, \quad (3)$$

$$CS_{MA} = \sigma_{3MA} = \sigma_{1A}/(d + 1), \quad (4)$$

The calculated in situ equivalent confining (CS_{MA}) and deviator (DS_{MA}) stresses at the Mogi line for Formation A can then be used to calculate the Brittle–Ductile State Parameter (χ) and the Brittle–Ductile Stress Index (I_{BD}) for Formation A according to the relationships provided in Equations (5) and (6):

$$\chi = (\sigma_1 - \sigma_3)^0_A - (\sigma_1 - \sigma_3)_{MA}, \quad (5)$$

$$I_{BD} = (\sigma_3^0 / \sigma_{3MA}), \quad (6)$$

where χ is the Brittle–Ductile State Parameter, which provides a measure of the distance to the Mogi line under conditions of constant confining stress, while I_{BD} provides a measure of the distance to the Mogi line under conditions of constant deviator stress.

Similarly, the Brittle–Ductile State Parameter (χ) and the Brittle–Ductile Stress Index (I_{BD}) can be calculated for Formation B's initial stress state shown in Figure 3, using Equations (3) to (6). A negative χ value indicates that the formation is in the ductile regime (based on its initial stress state), whereas a positive χ value indicates that the formation is in the brittle regime (based on its initial stress state). Values of I_{BD} of one or below indicate that the initial stress state of the formation is within range of the brittle–ductile transition state, while (I_{BD}) values of greater than one indicate that the initial stress state of the formation is further away from the brittle–ductile transition state.

2.4. Estimation of the In Situ Stress State of Each Major Injection and Confining Formation in the Alberta Basin

An extensive database of in situ vertical and minimum horizontal stress measurements exists for various formations of interest to the hydrocarbons, disposal and cavern storage industries in Alberta. Density logs are routinely collected to meet operational and regulatory requirements in the hydrocarbon industry, and integration of these logs to the depth of interest provides a reliable estimate of the vertical stress (gradient) at the target zone [46]. Mini-fracture tests (also referred to as minifrac, diagnostic fracture injection tests or DFITs) required for operational (e.g., fracture design [47]) and regulatory (e.g., AER's Directive 40 [48]) requirements typically provide reliable estimates of the magnitude of the in situ minimum horizontal stress [49]. Formation pressure tests are routinely conducted to meet operational and regulatory requirements and can provide reliable estimates of the formation pore pressure (gradients) for most formations in the Alberta Basin [4]. Additional sources of minifrac, vertical stress and pore pressure data include the published reports listed in the Data Availability section.

While comprehensive vertical, minimum horizontal stress and pore-pressure data are publicly available for many formations in the Alberta Basin, these data are widely distributed across many different sources, such as regulatory, industry, academic and scientific publications. We consolidated the vertical, minimum horizontal stress and pore pressure data contained in the publications listed in the Data Availability section into a single Excel database and then used this database to compute the complete stress state of the individual formations using the methods described below. In approximately 30% of the cases, UWIs were provided, but the corresponding formations were not listed. In such cases, geological interpretation of the specific well logs was required to identify each corresponding formation for the in situ stress/pore pressure measurements. Additionally, data vintages varied widely, with relatively recent data available for formations of interest to the tight (e.g., the Montney and Duvernay) and thermal (e.g., Clearwater caprock, McMurray reservoir) hydrocarbons industries, while data for other (e.g., deep carbonate) formations were collected up to several decades ago.

Determination of the Brittle–Ductile State Parameter (χ) and the Brittle–Ductile Stress Index (I_{BD}) requires the full stress tensor (i.e., σ_1 , σ_2 and σ_3). The frictional limits theorem can be used to estimate the upper limit of the magnitude of the maximum horizontal stress (i.e., σ_1) under (critically stressed) reverse and strike-slip faulting conditions, which are responsible for the occurrence of felt-induced seismicity in the Alberta Basin [50]. This theorem assumes that the maximum horizontal stress is horizontal and is limited by the frictional strength of faults within the rock mass, as shown in Equations (7) and (8) below [51,52]:

$$\sigma_{1 \max} = f(\mu) * (\sigma_3 - P_p) + P_p, \quad (7)$$

$$f(\mu) = [(1 + \mu^2)^{1/2} + \mu]^2, \quad (8)$$

where μ is the coefficient of internal friction and P_p is the formation pore pressure. The coefficient of internal friction is the tangent of the angle of internal friction of the formation core sample (i.e., $\tan(\varphi)$) and is calculated from the formation core triaxial test database, while formation pore pressure and minimum stress measurements (which can be either horizontal or vertical) are available from the in situ test database compiled above. Therefore, assuming that geologic faults are present and in a critically stressed state, the complete in situ stress state of each formation can be estimated using Equations (7) and (8), in conjunction with the measured in situ stress (i.e., vertical stress, minimum horizontal stress and pore pressure) and the triaxial test database. Critically stressed faults appear to be prevalent across all continental regions [1], and direct/indirect triggering of such faults has been the main causal factor for fluid-injection-induced seismicity in this basin [53].

Ranges of minimum horizontal stress and pore pressure (gradient) measurements were available for individual formations, depending on the characteristics of the lithology, location, measurement method and vintage of the data. The minimum and maximum stress and pore pressure measurements for each formation were used to create a low and a high range of minimum horizontal stress, vertical stress and formation pore pressure for the corresponding depth range of each formation. The combinations of low and high σ_3 , σ_v and P_p values were then used to calculate the corresponding maximum horizontal stress for each scenario, resulting in a minimum and maximum value for each of σ_1 , σ_2 , σ_3 and P_p at the corresponding formation depth. Only reverse ($\sigma_v = \sigma_3$) and strike-slip ($\sigma_v = \sigma_2$) stress regimes have been considered in this analysis since only these cases have been linked to the occurrence of felt-induced seismicity in the Alberta Basin [8,50,54–56].

This approach resulted in four possible combinations of confining stress ($CS = \sigma_3$) and deviator stress ($DS = \sigma_1 - \sigma_3$) that could be used to calculate the Brittle–Ductile State Parameter (χ) and the Brittle–Ductile Stress Index (I_{BD}). These are (i) a high CS-high DS (HCS-HDS), (ii) a high CS-low DS (HCS-LDS), (iii) a low CS-high DS (LCS-HDS) and (iv) a low CS-low DS (LCS-LDS). The use of the LCS-HDS combination minimizes both the Brittle–Ductile State Parameter (χ) and the Brittle–Ductile Stress Index (I_{BD}) for each formation, and this combination was used as the default (conservative case) analysis scenario. This scenario is also consistent with the observations of previous work, which noted that low confining stress (and high deviator stress) in deep carbonate formations is associated with an increased probability of induced seismicity occurrence in the Alberta Basin [18].

3. Results

In the sub-sections below, we used the data analyzed to identify the geologic formations most utilized for fluid injection in the Alberta Basin. We also presented the (calculated) modified Mogi ductility (d^*) parameter to evaluate the relative brittleness/ductility of these formations and to identify the most brittle and most ductile injection and confining formations in this basin. We then used our Brittle–Ductile State (χ) and Brittle–Ductile Stress Index (I_{BD}) parameters and the measured in situ stress reported in the existing literature to evaluate the brittleness of the major injection formations at the time of in situ data collection.

3.1. Major Injection Formations in the Alberta Basin

Table 2 below presents the summary of major injection formations identified in the Alberta Basin and the relative proportion of fluid volumes (measured at surface conditions) injected into each type of formation.

Table 2 shows that approximately 94% of the water, 88% of the gases and 100% of the steam that have been injected into the Alberta Basin over the past six decades were injected into 27 major formations. Most of these fluids were injected into three Lower Cretaceous sandstones and nine Devonian carbonate hydrocarbon reservoirs that were extensively exploited, resulting in significant historical formation pressure depletion [4]. These formations are located at intermediate depths, generally sandwiched between extensive regional low permeability (confining) formations, and possess the geologic characteristics required

to isolate injected fluid from both the ground surface and the Precambrian basement. These carbonate-rich formations, along with their confining geologic units (generally low permeability shales or mudstones), form the focus of the subsequent geomechanical data analyses provided in this study.

Table 2. Geologic formations receiving the largest volumes of injected fluids in the Alberta Basin and the relative proportion of fluid volumes (measured at surface conditions) injected over the period January 1960 to December 2021. Steam injected is reported in cold-water equivalent volumes at surface conditions.

Geologic Formation	Water Injected ¹	Gas Injected ¹	Steam Injected ¹
Paleogene sands (Swan Hills)	17.1%	14.0%	0%
Lower Cretaceous sandstones (McMurray, Clearwater, Cardium, Viking, Nikanassin)	30.6%	9.8%	97.9%
Jurassic sandstones (Sawtooth)	11.5%	15.1%	0%
Triassic carbonates (Charlie Lake, Halfway)	0.4%	1.0%	0%
Triassic siltstones (Montney, Doig)	0.3%	0.6%	0%
Permian sandstones (Belloy)	0.2%	0%	0%
Carboniferous carbonates (Banff, Debolt, Elkton, Livingston, Turner Valley)	0.7%	1.8%	0%
Devonian carbonates (Arcs, Grosmont, Keg River, Leduc, Muskeg, Nisku, Slave Point, Wabamun, Winterburn)	29.2%	43.3%	1.4%
Devonian sandstones (Granite Wash, Gilwood)	4.1%	0.6%	0%
Cambrian sandstones (Basal Sandstone Unit)	0.3%	0%	0.8%
Total volumes injected in above-listed formations	23.8 km ³	596.7 km ³	3.41 km ³
Total fluid volumes injected into all formations in the Alberta Basin	25.2 km ³	692.2 km ³	3.41 km ³

¹ Totals may not add to 100% due to rounding. Fluid volumes are reported in cubic kilometers (i.e., km³ = cubic kilometers).

Notably, Table 2 does not account for the geographic extent of the listed formations and consequently for differences in the geographic distribution of the injection fluid volumes. For instance, the Cretaceous, Devonian and Triassic formations listed are geographically extensive, present in most of the Alberta Basin, and the fluid volumes injected are correspondingly geographically distributed [4]. Conversely, the (regional) Permian (e.g., Belloy) and Carboniferous carbonate (e.g., Debolt) formations have a limited geographic distribution with injection volumes concentrated in specific areas. Despite the apparent marginal contribution at a basin scale, at a regional scale these formations support large volumes of industrial-scale fluid injection activities, especially over the last decade (Figure 4).

As shown in Figure 4, fluid injection into some of these regional disposal formations has increased notably over the last decade, as the hydrocarbon industry in Alberta and the types of subsurface activities conducted in its subsurface have evolved. Significant future increase in fluid injection volumes in these regional formations is expected over the next decade to support energy transition and net zero energy objectives [4], which has the potential to considerably alter the stress and pore pressure states of these formations.

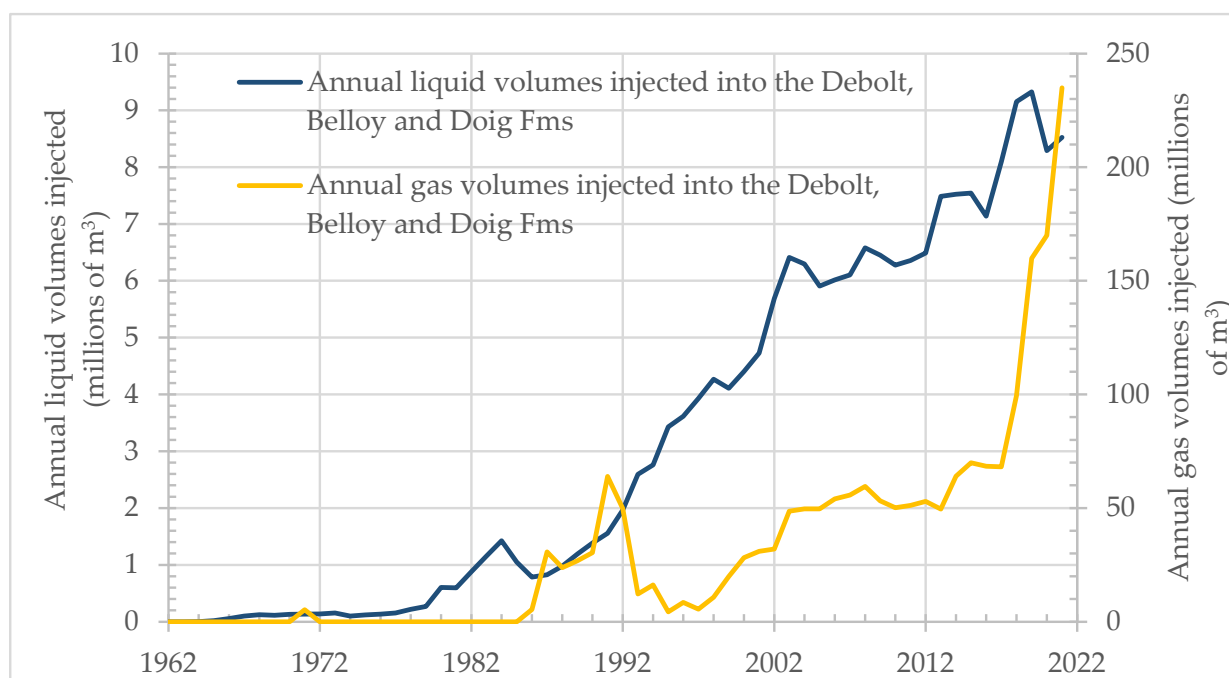


Figure 4. Annual fluid volumes (measured at surface conditions) injected into three regional (i.e., limited geographic extent) formations in the Alberta Basin.

3.2. Determination of the Mogi Brittle–Ductile State Limits and Relative Brittleness of Major Injection and Confining Formations in the Alberta Basin

Table 3 below presents the summary of the laboratory-measured geomechanical properties used to calculate the empirical (d) and modified (d^*) Mogi ductility parameters.

The empirical Mogi ductility parameter (d) for formations in the Alberta Basin (Table 3) indicates that most of the 51 formations evaluated are relatively ductile, which (in combination with extensive basin-wide pressure depletion [4]) may help to explain the relative success of sustained historical high-volume fluid injection in this basin [57]. Approximately 72% of the empirical ductility values in Table 3 are significantly higher than the typical ranges reported for similar types of rocks in the existing literature (e.g., Walton, 2021). Walton (2021) noted that silicate rocks tend to have d values in the range of 0.9–4.1, while the d values of carbonate-based rocks range from 3.5 to 10.7 (in the case of marble). The higher d values of rocks in the Alberta Basin are likely a function of the high carbonate content, porosity and heterogeneity of its lithological sequences compared to those reported in the literature. For instance, the limestone/dolomite content of the Alberta Basin sandstone core samples presented in Table 3 ranged from 5% to more than 30%, whereas the Berea sandstone samples referenced in the published literature [42] only contained up to 2% dolomite [58] (i.e., far less than that of the Alberta Basin sandstones). Additionally, carbonate presence was pervasive in all core sample results examined, with limestone/dolomite content ranging from 5% to above 80%. Secondary porosity is also likely a significant contributing factor to the higher d values in the Alberta Basin since the degree of faulting and fracturing is directly correlated to the ductility of (dolomitic) rocks under conditions of high confining pressure [59]. The injection formations listed above are all depleted hydrocarbon reservoirs, which have elevated secondary porosity and pervasive dolomitic mineral content (in the core samples tested, as shown in Table 3). Geological heterogeneity in the Alberta Basin is also high, with most of the core samples contained in Table 3 consisting of layered, interbedded lithological sequences and mixed clastic rock types, which is unique compared to the (relatively homogeneous) samples tested and results reported in the existing literature in this field.

Table 3. Summary of laboratory triaxial test data, empirical and modified Mogi ductility parameter for major injection and confining formations in the Alberta Basin.

Formation *	No. of Wells	No. of Core Tests	Major Core Lithology	TVD from (m)	TVD to (m)	Mean UCS (MPa)	Mean n (%)	Mean ϕ	Mean μ	σ_1 (MPa)	σ_3^* (MPa)	d	d*
Lea Park ^{2,4}	1	6	Clayey shale	1524	1531	0.04	13	28	0.5	38	18	1.1	28.9
Cardium ^{3,4}	4	21	Sandstone, carbonate cement	1794	2477	49	5	37	0.8	184	19	8.5	0.17
Second White Specks ^{2,3,4}	11	194	Calcareous siltstone	323	2782	79	3	31	0.6	252	42	5.0	0.06
Fish Scales ^{2,4}	1	12	Silty shale	469	471	15	21	32	0.6	25	5	4.5	0.30
Dunvegan ^{3,4}	1	16	Dolomitic siltstone	1751	1823	224	5	38	0.8	185	10	17.0	0.08
Viking ^{3,4}	3	28	Calcareous sandstone	507	2182	39	19	37	0.8	133	23	4.8	0.12
Joli Fou ^{2,4}	2	11	Silty shale	287	599	19	16	25	0.5	4	1	2.5	0.13
Falher G, H ^{3,4}	1	56	Silica cemented sandstone	2928	3064	107	8	33	0.7	312	42	6.4	0.06
Upper Clearwater ^{2,4}	10	73	Silty shale	96	243	2	35	28	0.5	7	3	1.3	0.61
Lower Clearwater ^{2,4}	24	154	Silty claystone, some siltstone	243	651	20	38	32	0.6	20	7	1.9	0.09
Spirit River ^{3,4}	1	18	Calcareous sandstone	2875	2892	93	9	33	0.6	234	27	7.7	0.08
Lower Mannville ^{3,4}	4	81	Calcareous sandstone	1398	2778	107	12	41	0.9	201	19	9.5	0.09
Ostracod ^{3,4}	4	8	Calcareous sandstone	2663	2692	131	4	40	0.8	276	26	9.6	0.07
Shallow Wilrich ^{2,4}	1	4	Silty clay shale	574	575	5	22	36	0.7	36	8	3.3	0.62
Deep Wilrich ^{2,3,4}	1	20	Argillaceous siltstone	2660	2695	137	3	38	0.8	279	40	6.0	0.04
Wabiskaw ^{3,4}	6	30	Silty mudstone	148	417	3	36	40	0.9	11	4	1.6	0.64
McMurray ^{3,4}	5	23	Weak sandstone	182	455	1	36	32	0.6	11	4	1.6	1.46
Nikanassin ^{3,4}	4	24	Sandstone	2280	3385	90	4	50	1.2	497	30	15.6	0.17
Fernie ^{2,4}	3	12	Calcareous shale	1845	3064	79	4	29	0.6	174	36	3.8	0.05
Nordeg ^{3,4}	12	95	Argillaceous limestone	1464	3079	149	4	38	0.8	214	34	5.2	0.03
Charlie Lake ^{2,3,4}	5	52	Dolomitic siltstone	1478	2241	85	12	52	1.3	206	18	10.4	0.12
Doig ^{3,4}	2	20	Dolomitic sandstone	2406	2990	59	4	53	1.3	224	18	11.2	0.19
Montney ^{2,3,4}	23	373	Dolomitic siltstone	823	3264	155	4	44	1.0	318	22	13.5	0.09
Belloy ^{3,4}	2	20	Dolomitic siltstone	2476	2672	164	9	44	1.0	316	42	6.5	0.04
Mt. Head ^{3,5}	1	8	Argillaceous limestone	2393	2405	108	6	40	1	417	37	10.3	0.10
Banff ^{2,3,5}	2	14	Dolomitic, silty mudstone	1550	1740	123	5	30	1	158	15	9.9	0.08
Exshaw ^{2,3,5}	3	19	Silty, argillaceous dolomite	1754	2419	179	3	48	1	313	23	12.4	0.07
Wabamun ^{1,3,5}	2	24	Micritic limestone	2238	2374	124	3	38	1	205	15	12.6	0.10
Ireton ^{1,2,5}	4	39	Calcareous shale	1594	3995	78	5	29	1	181	20	8.1	0.10
Leduc ^{1,3,5}	2	20	Vuggy dolostone	1618	1851	103	6	48	1	214	17	11.4	0.11
Duvernay Innisfail ^{1,2,3,5}	2	22	Calcareous, silty mudstone	1819	2017	100	8	33	1	175	22	7.0	0.07

Table 3. Cont.

Formation *	No. of Wells	No. of Core Tests	Major Core Lithology	TVD from (m)	TVD to (m)	Mean UCS (MPa)	Mean n (%)	Mean ϕ	Mean μ	σ_1 (MPa)	σ_3^* (MPa)	d	d*
Duvernay Kaybob ^{2,3,5}	22	599	Calcareous silty mudstone	2274	4070	71	8	40	1	164	14	10.9	0.15
Duvernay W. Green ^{2,3,5}	15	122	Calcareous mudstone	2796	3524	44	5	41	1	138	10	12.8	0.29
Majeau Lake ^{1,2,5}	1	22	Calcareous shale	3233	3439	76	7	36	1	187	40	3.7	0.05
Muskwa ^{1,2,5}	5	32	Calcareous, silty shale	1459	2190	73	8	43	1	78	10	6.9	0.10
Waterways ^{2,5}	3	13	Calcareous shale	498	767	69	4	49	1	80	5	15.0	0.22
Slave Point ^{3,5}	7	60	Micritic limestone	324	1366	81	6	43	1	181	5	35.3	0.43
Fort Vermillion ^{2,5}	3	31	Anhydrite, interbedded calcareous shale	402	778	112	3	47	1	186	10	17.6	0.16
Watt Mt. ^{3,5}	11	165	Anhydrite, interbedded siltstone, dolomite	343	2198	79	0	42	1	124	9	13.2	0.17
Muskeg ^{2,5}	3	17	Dolomite, interbedded shales	739	1523	78	4	44	1	85	5	15.9	0.20
Keg River ^{3,5}	6	49	Dolomite, interbedded anhydrite	1014	1778	104	3	50	1	175	20	7.8	0.07
Contact Rapids ^{2,5}	5	54	Calcareous mudstone	1012	1814	76	7	51	1	123	15	7.2	0.09
Cold Lake Limestone ^{2,5}	2	16	Clastic limestone	1383	1796	156	3	41	1	322	15	20.5	0.13
Cold Lake Shale ^{2,5}	3	36	Argillaceous dolostone	956	1830	85	4	40	1	132	16	7.1	0.08
Ernestina Lake Anhydrite ^{2,5}	10	138	Calcareous, silty anhydrite	1068	1132	136	0	32	1	194	10	18.4	0.14
Ernestina Lake Limestone ^{2,5}	10	88	Calcareous, argillaceous limestone	963	1837	78	0	42	1	111	10	10.1	0.13
Basal Red Beds ^{3,5}	1	16	Calcareous siltstone, anhydrite stringers	1494	1609	92	6	42	1	86	5	16.2	0.18
Basal Sandstone Unit ^{3,5}	5	51	Fine grained, calcareous sandstone	2050	2732	45	14	42	1	123	11	10.5	0.23

* Only formations for which multi-stress triaxial testing data were available are listed. ¹ Poor confining stress resolution. ² Confining formation. ³ Injection formation. ⁴ Mesozoic-era formation. ⁵ Paleozoic-era formation. "TVD from" and "TVD to" indicate sampling location depth intervals. TVD: total vertical depth from ground surface.

Analysis of the d* values in Table 3 shows that the Upper Clearwater, Lea Park and shallow Wilrich shales appear to be the most ductile, whereas the lower Clearwater and the Joli Fou appear to be the most brittle of the confining sequences in the Mesozoic era. Examination of the d* values for Mesozoic-era formations also suggests that the Nordegg, Belloy, Deep Wilrich and Falher appear to be the most brittle injection formations in this era, while the most ductile injection formations of this era appear to be the Wabiskaw/McMurray, Doig, Cardium and Nikanassin. Examination of the d* values of formations in the Paleozoic era indicates that the Majeau Lake, Exshaw, Duvernay Innisfail and Keg River appear to be the most brittle injection formations, whereas the Slave Point, Duvernay Willesden Green, Basal Sandstone Unit, and Basal Red Beds appear to be the most ductile formations of this era.

An analysis of the current Brittle–Ductile State Parameter and the Brittle–Ductile Stress Index (using the current site-specific in situ stress conditions relative to the respective Mogi line) is required to assess the probability that such formations within the area of interest of

a fluid injection project could be brittle/ductile under the current in situ stress conditions. Such an analysis would involve collecting current in situ stress and pore pressure data from lithological sequences at sites of interest and then calculating the Brittle–Ductile State Parameter (χ) and the Brittle–Ductile Stress Index (I_{BD}) to assess the site-specific brittle–ductile state of the stratigraphic sequences at each site. We use the historical stress and pore pressure data available for formations in the Alberta Basin in the section below to calculate the last-known brittle–ductile state of each formation in order to demonstrate the utility of our conceptual framework.

3.3. Determination of the Brittle–Ductile State Parameter and Brittle–Ductile Stress Index for Major Injection Formation and Confining Sequences in the Alberta Basin

Table 4 below shows the calculated historical Brittle–Ductile State Parameter (χ) and the Brittle–Ductile Stress Index (I_{BD}) for major injection and confining formations in the Alberta Basin. Since the χ and I_{BD} provided below are based on the formation stress state at the time of the in situ and pore-pressure data collection (using the LCS-HDS scenario), the formation regime provided in Table 4 below is only applicable for the geographic location and period in which the minifrac data were collected. Regional changes in the net fluid balance have been occurring in specific formations and regions in this basin over the last decade, and such activity can alter formation stresses. Therefore, current site-specific in situ stress data are required to assess the current brittle–ductile state of stratigraphic sequences, and site-specific multi-stress triaxial core analyses are required to account for site-specific geological heterogeneities that may exist within the project area of interest. Additionally, this list does not include formations for which insufficient in situ stress and pore pressure data were available at the time of this analysis.

Table 4 indicates that only 4 (Lea Park, Upper Clearwater, Wabiskaw and McMurray) of the 41 major injection and confining formations assessed in the Alberta Basin appeared to be in the brittle regime, while all others were in a ductile regime (under an LCS-HDS scenario) at the time of data collection. This is somewhat expected since brittleness has been previously reported in the Clearwater shales [60] and shaly sections of the Wabiskaw Formation [61], whereas brittle behavior is typical of the locked sands of the McMurray Formation [62,63]. However, this analysis also suggests that some major injection/confining formations, such as the Belloy, Doig, Muskwa, Majeau Lake, Duvernay Innisfail, Shallow and Deep Wilrich, Joli Fou and Fish Scales, could be close to a brittle state (at the time of the in situ stress and pore pressure measurements). Additionally, this analysis indicates that the Duvernay Willesden Green could be considerably more ductile than the Kaybob and Duvernay Innisfail, which offers additional insights into the relative seismic quiescence [64] of the former and the seismogenicity [40] of the latter formation sequences when subjected to high volume fluid injection.

As shown in Table 4, the vintage of the in situ stress measurements used in this assessment varies significantly, ranging from data collected in the late 1970s up to 2019. Most of the earlier data were collected for basin-wide stress and acid-gas storage studies, whereas most of the recent in situ stress and pore pressure data available was obtained from low permeability formations (collected for hydraulic fracturing design or thermal caprock characterization purposes). Over this period, extensive fluid extraction and injection activities occurred in this basin, with large-scale fluid extraction resulting in regional formation depletion in most areas and, in some areas, large-scale injection resulting in local formation pore pressure increase [4]. Large-scale fluid injection can lead to formation pore pressure (and temperature) changes, cause formation deformation, and substantially alter total formation stresses in every direction [65]. Therefore, an assessment of the current brittle/ductile state of a formation using our method described above requires an assessment of the current in situ stress state of the formations of interest. Consequently, while our assessments in Table 4 provide the brittle–ductile state of the formations at the time of (in situ stress) data collection, continuous and evolving injection and production activity occurring within this basin are likely to have altered the stress state in these formations. However, current site-specific (in situ stress, pore pressure, geological and geomechanical) data collection is typically required to support the project design, risk assessment and regulatory application process for fluid injection projects. The use of our method, in conjunction with such

site-specific and recent data, can provide an assessment of the current brittle–ductile state of the formations of interest and the potential for seismic/aseismic slip in hosted faults.

Table 4. Assessment of the Brittle–Ductile State (χ) and Brittle–Ductile Stress Index (I_{BD}) of major formations in the Alberta Basin (at the time of in situ stress and pore pressure data measurements and under the LCS-HDS scenario).

Formation ¹	TVD (m)	d	Max In Situ σ_1 (MPa)	Min In Situ σ_3 (MPa) ⁴	Year Minifrac Data Collected	Max In Situ DS (MPa)	DS on Mogi Line (MPa)	CS on Mogi Line (MPa)	χ (MPa)	I_{BD}	Formation Regime ³
Lea Park	325	1.1	15.6	6.8	2011	9	7	7	1	0.9	Brittle
Cardium	2742	8.5	147.4	34.3	2012	113	291	16	−178	2.2	Ductile
Second White Specks	3300	5.0	123.3	54.5	2011	69	272	21	−203	2.7	Ductile
Fish Scales	1644	4.5	82.3	26.9	2011	55	121	15	−66	1.8	Ductile
Dunvegan	1974	17.0	85.6	27.9	2016 ²	58	474	5	−416	5.9	Ductile
Viking	2875	4.8	153.5	39.1	2019	114	188	26	−73	1.5	Ductile
Joli Fou	750	2.5	29.7	13.5	2019	16	34	8	−18	1.6	Ductile
Falher G, H	2147	6.4	65.5	30.9	2016 ²	35	198	9	−163	3.5	Ductile
Upper Clearwater	304	1.3	15.4	4.6	2019	11	6	7	5	0.7	Brittle
Spirit River	2892	7.7	110.0	34.4	2019	76	265	13	−189	2.7	Ductile
Lower Mannville	2510	9.5	124.1	29.9	2019	94	284	12	−189	2.5	Ductile
Ostracod, Ellerslie	3005	9.6	131.5	46.3	2016 ²	85	444	12	−359	3.7	Ductile
Shallow Wilrich Shale	575	3.3	33.8	8.3	2019	25	27	8	−2	1.1	Ductile
Deep Basin Wilrich	2695	6.0	168.7	38.8	2016 ²	130	231	24	−101	1.6	Ductile
Wabiskaw	194	1.6	17.7	2.3	2019	15	4	7	12	0.3	Brittle
McMurray	291	1.6	16.0	3.4	2019	13	6	6	7	0.6	Brittle
Nikanassin	3211	15.6	143.9	43.8	2016 ²	100	682	9	−582	5.0	Ductile
Fernie	2429	3.8	84.9	38.9	2016 ²	46	148	18	−102	2.2	Ductile
Nordegg	3093	5.2	125.3	47.3	2016 ²	78	246	20	−168	2.3	Ductile
Charlie Lake	1487	10.4	111.3	29.0	2005 ²	82	301	10	−219	3.0	Ductile
Doig	2358	11.2	382.4	37.5	2004 ²	345	421	31	−76	1.2	Ductile
Montney	2987	13.5	113.7	41.2	2018	73	556	8	−484	5.3	Ductile
Belloy	1940	6.5	194.2	30.5	2004 ²	164	198	26	−34	1.2	Ductile
Mount Head	2393	10.3	189.7	43.3	2004 ²	146	445	17	−298	2.6	Ductile
Banff	1550	9.9	74.7	29.5	2016 ²	45	291	7	−245	4.3	Ductile
Exshaw Limestone/Shale	3066	12.4	230.1	58.3	2004 ²	172	720	17	−548	3.4	Ductile
Wabamun	3822	12.6	178.8	52.0	2005 ²	127	655	13	−528	4.0	Ductile
Ireton	2542	8.1	81.6	39.7	2016 ²	42	321	9	−279	4.4	Ductile
Leduc	2677	11.4	161.3	37.0	2000	124	420	13	−296	2.8	Ductile
Duvernay Innisfail	1964	7.0	85.6	27.9	2019	58	194	11	−136	2.6	Ductile
Duvernay Kaybob	3442	10.9	142.5	50.5	2019	92	549	12	−457	4.2	Ductile
Duvernay Willesden Green	3800	12.8	103.1	64.6	2019	38	827	7	−788	8.6	Ductile
Majeau Lake	3916	3.7	104.0	57.4	2002	47	211	22	−164	2.6	Ductile
Muskwa	1565	6.9	97.8	20.8	2016 ²	77	144	12	−67	1.7	Ductile
Waterways	2197	15.0	161.1	38.0	2016 ²	123	570	10	−447	3.8	Ductile
Slave Point	1500	35.3	59.5	18.3	2014 ²	41	646	2	−604	11.2	Ductile
Watt Mountain	2198	13.2	139.3	33.5	1982	106	441	10	−335	3.4	Ductile
Muskeg	1905	15.9	128.8	29.0	2013	100	462	8	−362	3.8	Ductile
Keg River/Winnepegosis	1531	7.8	56.4	24.6	2016 ²	32	192	6	−161	3.8	Ductile
Basal Red Beds	1194	16.2	82.4	18.7	2009	64	304	5	−240	3.9	Ductile
Basal Sandstone Unit	2669	10.5	188.2	45.2	2009	143	475	16	−332	2.8	Ductile

¹ Only formations with available in situ stress data are listed. ² Indicates year stress data was published; actual date of stress data collection was sometime between late 1970 and 2015. ³ At time/location of the in situ stress data collection. ⁴ Lowest measured confining stress for formation.

4. Discussion

Aseismic creep has been postulated to be the main process driving natural earthquake swarms in shallow strike-slip faults globally, with interconnected vertically stacked creep and dynamic rupture (brittle failure) processes responsible for seismogenicity in some major faults such as the San Andreas [66]. Most of the world's seismicity in sedimentary cover occurs in carbonate sequences, driven by fault creep and rupture, which transitions from slow, stable (ductile) slip to rapid unstable (stick; brittle) slip at confining stresses above in situ conditions typically present at depths of 3–5 km (i.e., temperatures above 65 °C and confining stresses above 60 MPa) [67]. This range of in situ conditions is analogous to those that exist in deep carbonaceous injection/confining formations of interest in the Alberta Basin (Table 4), in which our proposed methods are anticipated to be applicable.

Shallow strike-slip faults are prevalent in the Alberta Basin, and swarm-type seismicity is characteristic of some of the major Alberta events triggered by fluid injection [68]. Aseismic creep in ductile formations triggering brittle faults within carbonate sequences has been postulated to be the main driver of fluid-injection-induced seismicity in this and other basins [33]. Current models for assessing and managing induced seismic risk may be inadequate in such cases since large events have been observed to occur outside the pressure influence zone and on faults considered not optimally oriented for slip (as in the case of the 12 January 2016, Mw 4.1 Fox Creek earthquake [7]). The faults on which the seismicity occurred in the Fox Creek case extended across most of the stratigraphic sequences, whereas the larger seismogenic events all occurred in the overlying (carbonate) Leduc Formation, while fault slip within the Kaybob Duvernay (shale injection) Formation was largely aseismic [69]. Aseismic slip has also been noted as a viable mechanism to explain the occurrence of recent far-field fluid-injection-induced seismic events in both Alberta and British Columbia, with aseismic slip occurring within the Montney and concurrent seismogenic slip in the underlying (carbonate) Belloy/Debolt formations [70,71].

Our analysis shows that (for an LCS-HDS stress scenario) the overlying Leduc (carbonate) Formation is more brittle ($\chi = -296$ MPa, $I_{BD} = 2.8$) than the underlying Kaybob Duvernay (shale) Formation ($\chi = -457$ MPa, $I_{BD} = 4.2$), and consequently more likely to host seismogenic fault slip (Table 4) within this stratigraphic sequence. In the case of seismic events triggered by hydraulic fracturing in Alberta and British Columbia, virtually all of the large induced seismic events triggered by injection into the (deep) Montney Formation ($\chi = -484$ MPa, $I_{BD} = 5.3$) were actually located in the underlying Belloy ($\chi = -34$ MPa, $I_{BD} = 1.2$) and Debolt (no data available) formations. Meanwhile, virtually all of the large induced seismic events triggered by stimulation activity in the Kaybob Duvernay ($\chi = -457$ MPa, $I_{BD} = 4.2$) were located in the overlying Leduc Formation ($\chi = -296$ MPa, $I_{BD} = 2.8$) [72]. Conversely, large-scale fluid injection occurring in the shallow Montney (i.e., outside of the zone of influence of the Belloy/Debolt) was observed to trigger (aseismic) slip equivalent to a Magnitude 5.0 earthquake, which resulted in measurable surface displacement but no detectable seismicity [71]. Our analysis indicates that such a response could be expected since both the Montney and Kaybob Duvernay are more ductile than the Belloy and Wabamun (under an LCS-HDS scenario; no data were available for the Debolt Formation; Table 4). Table 5 below shows that the major fluid-injection-induced seismic events that have occurred to date in Alberta and British Columbia have occurred in the most brittle (underlying/overlying) formation(s) in the stratigraphic sequence adjacent to the fluid injection zone.

Therefore, aseismic slip increasing the stress in and triggering brittle failure in faults hosted in more brittle formations adjacent to the injection zone may be a likely contributing mechanism in the cases outlined above. Our analysis provides a method to identify the relative brittleness of injection and confining formations and to assess the potential for brittle failure to occur by computing and comparing the Brittle–Ductile State Parameter (χ) and Brittle–Ductile Stress Index (I_{BD}) in each formation in the stratigraphic sequence of interest. While our method requires current site-specific in situ stress and pore pressure data for each major stratigraphic sequence in the zone of influence of injection projects, such measurements are routinely collected as a part of injection project design regulatory

requirements in Alberta. Table 6 shows the four major formations closest and furthest from the brittle state at the time of the in situ stress and pore pressure measurements, which may help guide data collection and hazard assessments for fluid injection projects proposed in these formations.

Table 5. Summary of recent significant induced earthquake sequences in Alberta and British Columbia.

Location (Year)	Largest Magnitude	Trigger Activity ¹	Injection Zone	Injection Zone d*	Earthquake Zone	Earthquake Zone d*
Musreau Lake (2018–2020)	3.9	WD [73]	Ireton	0.10	Nisku Precambrian	ND ND ²
Peace River (2018–2020)	3.2	WD [8]	Leduc	0.11	Leduc Precambrian	0.11 ND ²
Red Deer (2019)	4.2	HF [8]	Duvernay Willesden Green	0.29	Leduc	0.11
Fox Creek (2016)	4.8	HF [8]	Kaybob Duvernay	0.15	Leduc	0.11
Fox Creek (2016)	4.1	HF [33]	Kaybob Duvernay	0.15	Wabamun Winterburn	0.10 ND
Cardston (2011–2012)	3.0	HF [74]	Exshaw	0.07	Wabamun Precambrian	0.10 ND ²
Cordel Field (1994–2008)	4.0	WD [75]	Turner Valley	ND	Turner Valley Precambrian	ND ND ²
Montney (2018) ³	4.45	HF [71,76]	Montney	0.09	Belloy Debolt	0.04 ND
Montney (2015) ³	4.55	HF [71]	Montney	0.09	Belloy	0.04
Montney (2015) ³	3.55	HF [71]	Montney	0.09	Belloy	0.04
Montney (2014) ³	3.9	HF [11]	Montney	0.09	Belloy	0.04
Montney (2013) ³	4.21	HF [71]	Montney	0.09	Belloy	0.04

¹ HF: Hydraulic fracturing. WD: Wastewater disposal. ² The igneous Precambrian basement is likely the most brittle formation in the stratigraphic sequence in the Alberta Basin. ³ Events located in British Columbia. ND: No data available.

Table 6. Alberta Basin injection and confining formations closest and furthest from the brittle state in situ (based on available historical in situ stress state and pore pressure measurements).

Geologic Era	Injection Formations Closest to Brittle State ¹	Injection Formations Furthest from Brittle State ¹	Confining Formations Closest to Brittle State ¹	Confining Formations Furthest from Brittle State ¹
Mesozoic	Wabiskaw-McMurray, Belloy, Viking, Doig	Nikanassin, Dunvegan, Ostracod-Ellerslie, Mannville	Clearwater, Lea Park, Wilrich, Joli Fou	Montney, Charlie Lake, Second White Specks, Fernie
Paleozoic	Muskwa, Keg River, Majeau Lake, Basal Red Beds	Slave Point, Wabamun, Muskeg, Watt Mountain	Banff, Exshaw, Ireton, Duvernay, Innisfail	Waterways, Duvernay, Willesden Green

¹ Some formations can be both injection and confining since high-volume fluid injection occurs in some confining (shale) formations for the purposes of tight hydrocarbon exploitation.

In the absence of current in situ stress and pore pressure data, the relative brittleness (d*) of the formation sequences in the fluid-injection project area of interest could provide

a screening-level indicator of the formations that are likely to be the most brittle in a stratigraphic sequence of interest. Table 7 provides the four most brittle and the four most ductile of the 51 (injection and confining) formations assessed in the Alberta Basin (based on d^* ; i.e., rock strength and material properties).

Table 7. Four most brittle and most ductile major injection and confining formations in the Alberta Basin, based on rock mechanical properties.

Geologic Era	Most Brittle Injection Formations ¹	Most Ductile Injection Formations ¹	Most Brittle Confining Formations ¹	Most Ductile Confining Formations ¹
Mesozoic	Nordeg, Belloy, Deep Wilrich, Falher G, H	Wabiskaw/McMurray, Doig, Cardium, Nikanassin	Deep Wilrich, Fernie, Second White Specks, Montney	Lea Park, Shallow Wilrich, Upper Clearwater, Fish Scales
Paleozoic	Majeau Lake, Exshaw, Duvernay, Innisfail, Keg River	Slave Point, Duvernay, Willesden Green, Basal Sandstone Unit, Basal Red Beds	Duvernay, Innisfail, Banff, Cold Lake Shale, Contact Rapids	Duvernay, Willesden Green, Waterways, Muskeg, Watt Mt.

¹ Some formations can be both injection and confining since high-volume fluid injection occurs in some confining (shale) formations for the purposes of tight hydrocarbon exploitation.

Triaxial core testing is considered a reasonable method of replicating stresses at reservoir conditions [77], but recovered core samples can be biased towards stronger and more competent zones within a stratigraphic sequence. Such more competent units are also more likely to be major stress-bearing members [78], display higher deviator stresses (i.e., high σ_1 and low σ_3), dominate the failure behavior of the rock unit and hosted faults and have been associated with an increased probability of fluid-injection-induced seismicity in the Alberta Basin [18]. However, while our analyses provides a regional-scale perspective of the brittle–ductile state of the stronger (more competent) formations within this basin, site-specific analyses of the stratigraphic sequences present would be required to account for project-scale geological heterogeneities. Additionally, the possibility exists that fault zones within dolomite layers may be even more brittle than the surrounding host rock since embrittlement and localization of brittle deformation of the fault core and the shear zone was previously noted [34]. This represents an area for future research.

Assessment of the potential for fluid injection projects to trigger seismicity has relied on the identification and avoidance of faults within the zone of influence [4]. However, assessment of the probability of aseismic slip within (more ductile) injection formations loading fault sections and triggering seismogenic slip in far-field, more brittle formations may be an important complement to the hazard assessment process for fluid injection projects. This complementary assessment may be especially important in the Alberta Basin since the types (strike-slip and reverse) of faults prevalent in this basin can be challenging to detect during the site selection process.

5. Conclusions

We provided an assessment of the relative brittleness/ductility of 51 of the major injection and confining formations in the Alberta Basin, as well as a method to assess the likelihood of a formation being in the brittle or ductile regime, using the current state of in situ stress and pore pressure.

This analysis indicates that approximately 72% of the formations had ductility significantly higher than typical ranges reported for similar-type rocks in the existing literature. The high ductility of the formations assessed, in conjunction with extensive historical pressure depletion, could be a contributing factor in the success of sustained historical high-volume fluid injection in this basin. However, some of the most brittle formations in

the stratigraphic sequences assessed include extensively used injection formations such as the Belloy, Deep Wilrich, Falher, Majeau Lake, Exshaw, Duvernay Innisfail and Keg River, and notable confining formations such as the Lower Clearwater and the Joli Fou shales. Increasing utilization of some of these injection formations (such as the Belloy and Doig) may require closer examination of their current/future brittle–ductile state to mitigate the potential for future seismogenesis.

Our analyses show that the Lea Park, Clearwater, Wabiskaw and McMurray formations were in a brittle state, and the Belloy, Doig, Muskwa, Majeau Lake, Duvernay Innisfail, Shallow and Deep Wilrich, Joli Fou and Fish Scales formations were close to the brittle state at the time the in situ stress data were collected. Almost all of the induced seismic events triggered by large-scale fluid injection into the (ductile-state) Montney formation in British Columbia occurred in the underlying (close to brittle state) Belloy and Debolt formations.

The data and method presented could be used to assess the potential for (sub)vertical fault sections to be aseismic/seismogenic by evaluating the relative brittleness/ductility and the in situ brittle/ductile state of host formations in the stratigraphic sequence of interest. Such information may be valuable during site selection for large-scale fluid injection projects by providing insight into the far-field seismogenic potential of unknown/undetected fault sections. Increasingly, it is recognized that near-field aseismic fault slip triggering far-field seismic fault slip is an important driving process for injection-induced seismicity both in the Alberta Basin (e.g., [33]) and globally (e.g., [79,80]).

Author Contributions: Conceptualization, M.S. and R.C.; methodology, M.S., R.C. and M.D.; software, M.S. and J.F.C.; validation, R.C., J.F.C. and M.D.; formal analysis, M.S.; investigation, M.S.; resources, H.C.; data curation, M.S. and J.F.C.; writing—original draft preparation, M.S.; writing—review and editing, R.C., M.D. and H.C.; visualization, M.S.; supervision, R.C. and H.C.; project administration, M.S. All authors have read and agreed to the published version of the manuscript.

Funding: This research received no external funding.

Data Availability Statement: In situ stress measurements are available from: (i) The Alberta Government's OpenData link, located at https://open.alberta.ca/opendata/gda-dig_2016_0040. (ii) Chapter 29 of the Atlas of the Western Canadian Sedimentary Basin, located at <https://ags.aer.ca/atlas-the-western-canada-sedimentary-basin/chapter-29-situ-stress>. (iii) AER/AGS Report 97 https://static.ags.aer.ca/files/document/REP/REP_97.pdf. (iv) AER/AGS Special Reports 090, 091, 092, 093, 094 & 095, all located at <https://ags.aer.ca/products/all-publications>. (v) AGS Digital Data 2018-0013, located at <https://ags.aer.ca/publication/dig-2018-0013>. (vi) Published reports and articles including [56,81–101]. Core-sample triaxial testing lab reports are available on request from the AER's data request catalog, located at <https://static.aer.ca/prd/documents/sts/GOS-REPS.xlsb>. Fluid-volume injection data are available from the geoSCOUT™ database located at www.geologic.com. All geoSCOUT data is © 2022. All hyperlinks were last accessed 4 July 2022.

Acknowledgments: The authors would like to acknowledge the Alberta Energy Regulator and the Alberta Geologic Survey for access to data, as well as the Alberta Department of Energy, the University of Alberta, and the University of Waterloo for the support provided over the course of this study. The authors would also like to thank the anonymous reviewers who helped to improve the quality of this paper.

Conflicts of Interest: The authors declare no conflict of interest.

References

1. Townend, J.; Zoback, M.D. How faulting keeps the crust strong. *Geology* **2000**, *28*, 399–402. [[CrossRef](#)]
2. Morell, K.D.; Styron, R.; Stirling, M.; Griffin, J.; Archuleta, R.; Onur, T. Seismic Hazard Analyses from Geologic and Geomorphic Data: Current and Future Challenges. *Tectonics* **2020**, *39*, e2018TC005365. [[CrossRef](#)]
3. Hough, S.E. Intraplate seismic hazard: Evidence for distributed strain and implications for seismic hazard. *Intraplate Earthq.* **2012**, 303–327. [[CrossRef](#)]
4. Samaroo, M.; Chalaturnyk, R.; Dusseault, M.; Jackson, R.; Buhlmann, A.; Custers, H. An Assessment of the Net Fluid Balance in the Alberta Basin. *Energies* **2022**, *15*, 1081. [[CrossRef](#)]
5. Ross, G.M.; Eaton, D.W. Basement reactivation in the Alberta Basin: Observational constraints and mechanical rationale. *Bull. Can. Pet. Geol.* **1999**, *47*, 391–411. [[CrossRef](#)]

6. Dietrich, J.R. Seismic stratigraphy and structure of the lower Paleozoic, Central Alberta Lithoprobe Transect. *Bull. Can. Pet. Geol.* **1999**, *47*, 362–374.
7. Eyre, T.S.; Eaton, D.W.; Zecevic, M.; D’Amico, D.; Kolos, D. Microseismicity reveals fault activation before Mw 4.1 hydraulic-fracturing induced earthquake. *Geophys. J. Int.* **2019**, *218*, 534–546. [[CrossRef](#)]
8. Schultz, R.; Wang, R. Newly emerging cases of hydraulic fracturing induced seismicity in the Duvernay East Shale Basin. *Tectonophysics* **2020**, *779*, 228393. [[CrossRef](#)]
9. Hope, J.; Eaton, D.W.; Ross, G.M. Lithoprobe seismic transect of the Alberta Basin: Compilation and overview. *Bull. Can. Pet. Geol.* **1999**, *47*, 331–345.
10. Schulte, B.W.M.; Lyatsky, H.; Bridge, D. Methods of fault detection with geophysical data and surface geology. *Can. J. Explor. Geophys.* **2019**, *44*, 1–23. Available online: <https://csegrecorder.com/articles/view/methods-of-fault-detection-with-geophysical-data-and-surface-geology> (accessed on 16 September 2022).
11. Bao, X.; Eaton, D.W. Fault activation by hydraulic fracturing in western Canada. *Science* **2016**, *354*, 1406–1409. [[CrossRef](#)]
12. Skoumal, R.J.; Ole Kaven, J.; Walter, J.I. Characterizing seismogenic fault structures in Oklahoma using a relocated template-matched catalog. *Seismol. Res. Lett.* **2019**, *90*, 1535–1543. [[CrossRef](#)]
13. Shah, A.K.; Keller, G.R. Geologic influence on induced seismicity: Constraints from potential field data in Oklahoma. *Geophys. Res. Lett.* **2017**, *44*, 152–161. [[CrossRef](#)]
14. Schultz, R.; Skoumal, R.J.; Brudzinski, M.R.; Eaton, D.; Baptie, B.; Ellsworth, W. Hydraulic fracturing-induced seismicity. *Rev. Geophys.* **2020**, *58*, 1–43. [[CrossRef](#)]
15. McGarr, A.; Barbour, A.J. Wastewater Disposal and the Earthquake Sequences during 2016 Near Fairview, Pawnee, and Cushing, Oklahoma. *Geophys. Res. Lett.* **2017**, *44*, 9330–9336. [[CrossRef](#)]
16. Hennings, P.H.; Nicot, J.P.; Gao, R.S.; DeShon, H.R.; Lund Snee, J.E.; Morris, A.P.; Brudzinski, M.R.; Horne, E.A.; Breton, C. Pore Pressure Threshold and Fault Slip Potential for Induced Earthquakes in the Dallas-Fort Worth Area of North Central Texas. *Geophys. Res. Lett.* **2021**, *48*, 1–9. [[CrossRef](#)]
17. Fan, Z.; Eichhubl, P.; Gale, J.F.W. Geomechanical analysis of fluid injection and seismic fault slip for the Mw 4.8 Timpson, Texas, earthquake sequence. *J. Geophys. Res. Solid Earth* **2016**, *121*, 3076–3095. [[CrossRef](#)]
18. Pawley, S.; Schultz, R.; Playter, T.; Corlett, H.; Shipman, T.; Lyster, S.; Hauck, T. The Geological Susceptibility of Induced Earthquakes in the Duvernay Play. *Geophys. Res. Lett.* **2018**, *45*, 1786–1793. [[CrossRef](#)]
19. Hincks, T.; Aspinall, W.; Cooke, R.; Gernon, T. Oklahoma’s induced seismicity strongly linked to wastewater injection depth. *Science* **2018**, *7911*, 1–46. [[CrossRef](#)]
20. Hui, G.; Chen, S.; Chen, Z.; Gu, F.; Ghoroori, M.; Mirza, M.A. Comprehensive Characterization and Mitigation of Hydraulic Fracturing-Induced Seismicity in Fox Creek, Alberta. *SPE J.* **2021**, *26*, 2736–2747. [[CrossRef](#)]
21. Sibson, R.H. Earthquake faulting as a structural process. *J. Struct. Geol.* **1989**, *11*, 1–14. [[CrossRef](#)]
22. Zhamaletdinov, A.A. *On the Nature of the Brittle-Ductile Transition Zone in the Earth’s Crust (Review)*; Springer International Publishing: Berlin/Heidelberg, Germany, 2019; Volume 2.
23. Brace, W.F.; Byerlee, J.D. Stick-Slip as a Mechanism for Earthquakes. *Science* **1966**, *153*, 990. [[CrossRef](#)]
24. Scholz, C.H. Earthquakes and friction laws. *Nature* **1998**, *391*, 37–42. [[CrossRef](#)]
25. Scholz, C.H. Brittle Tectonics: A Non-linear Dynamical System. In *Encyclopedia of Complexity and Systems Science*; Myers, R., Ed.; Springer: Berlin/Heidelberg, Germany, 2009; Volume 1, pp. 657–674.
26. Byerlee, J.D.; Brace, W.F. High Pressure Mechanical Instability in Rocks. *Science* **1969**, *164*, 713–716. [[CrossRef](#)]
27. Bürgmann, R.; Dresen, G. Rheology of the lower crust and upper mantle: Evidence from rock mechanics, geodesy, and field observations. *Annu. Rev. Earth Planet. Sci.* **2008**, *36*, 531–567. [[CrossRef](#)]
28. Jolivet, R.; Simons, M.; Agram, P.S.; Duputel, Z.; Shen, Z.K. Aseismic slip and seismogenic coupling along the central San Andreas Fault. *Geophys. Res. Lett.* **2015**, *42*, 297–306. [[CrossRef](#)]
29. Abdelmeguid, M.; Elbanna, A. Sequences of seismic and aseismic slip on bimaterial faults show dominant rupture asymmetry and potential for elevated seismic hazard. *Earth Planet. Sci. Lett.* **2021**, *593*, 117648. [[CrossRef](#)]
30. Hirth, G.; Beeler, N.M. The role of fluid pressure on frictional behavior at the base of the seismogenic zone. *Geology* **2015**, *43*, 223–226. [[CrossRef](#)]
31. Aubry, J.; Passelègue, F.X.; Escartín, J.; Gasc, J.; Deldicque, D.; Schubnel, A. Fault Stability Across the Seismogenic Zone. *J. Geophys. Res. Solid Earth* **2020**, *125*, 1–21. [[CrossRef](#)]
32. Vajdova, V.; Zhu, W.; Natalie Chen, T.M.; Wong, T.F. Micromechanics of brittle faulting and cataclastic flow in Tavel limestone. *J. Struct. Geol.* **2010**, *32*, 1158–1169. [[CrossRef](#)]
33. Eyre, T.S.; Eaton, D.W.; Garagash, D.I.; Zecevic, M.; Venieri, M.; Weir, R.; Lawton, D.C. The role of aseismic slip in hydraulic fracturing-induced seismicity. *Sci. Adv.* **2019**, *5*, 1–11. [[CrossRef](#)]
34. De Paola, N.; Colletini, C.; Faulkner, D.R.; Trippetta, F. Fault zone architecture and deformation processes within evaporitic rocks in the upper crust. *Tectonics* **2008**, *27*, 1–21. [[CrossRef](#)]
35. Brantut, N.; Schubnel, A.; Rouzaud, J.N.; Brunet, F.; Shimamoto, T. High-velocity frictional properties of a clay-bearing fault gouge and implications for earthquake mechanics. *J. Geophys. Res. Solid Earth* **2008**, *113*, 1–18. [[CrossRef](#)]
36. Mews, K.S.; Alhubail, M.M.; Barati, R.G. A Review of Brittleness Index Correlations for Unconventional Tight and Ultra-Tight Reservoirs. *Geosciences* **2019**, *9*, 319. [[CrossRef](#)]

37. Schultz, R.; Corlett, H.; Haug, K.; Kocon, K.; McCormack, K.; Stern, V.; Shipman, T. Linking fossil reefs with earthquakes: Geologic insight to where induced seismicity occurs in Alberta. *Geophys. Res. Lett.* **2016**, *43*, 2534–2542. [CrossRef]
38. Ehrenberg, S.N.; Nadeau, P.H. Sandstone vs. carbonate petroleum reservoirs: A global perspective on porosity-depth and porosity-permeability relationships. *Am. Assoc. Pet. Geol. Bull.* **2005**, *89*, 435–445. [CrossRef]
39. Kurzawski, R.M.; Stipp, M.; Niemeijer, A.R.; Spiers, C.J.; Behrmann, J.H. Earthquake nucleation in weak subducted carbonates. *Nat. Geosci.* **2016**, *9*, 717–722. [CrossRef]
40. Schultz, R.; Atkinson, G.; Eaton, D.W.; Gu, Y.J.; Kao, H. Hydraulic fracturing volume is associated with induced earthquake productivity in the Duvernay play. *Science* **2018**, *359*, 304–308. [CrossRef] [PubMed]
41. McGarr, A.; Simpson, D.; Seeber, L. 40 Case histories of induced and triggered seismicity. In *International Geophysics*, 81st ed.; Lee, W.H.K., International Association of Seismology and Physics of the Earth's Interior, Committee on Education, International Association for Earthquake Engineering, Eds.; Academic Press: Cambridge, MA, USA, 2002; Volume 81, pp. 647–661.
42. Walton, G. A New Perspective on the Brittle–Ductile Transition of Rocks. *Rock Mech. Rock Eng.* **2021**, *54*, 5993–6006. [CrossRef]
43. Hajiabdolmajid, V.; Kaiser, P.K.; Martin, C.D. Modeling brittle failure of rock. *Int. J. Rock Mech. Min. Sci.* **2002**, *34*, 227–244. [CrossRef]
44. Mogi, K. Pressure dependence of rock strength and transition from brittle fracture to ductile flow. *Bull. Earthq. Res. Inst.* **1966**, *44*, 215–232. Available online: https://repository.dl.itc.u-tokyo.ac.jp/record/33594/file_preview/ji0441012.pdf (accessed on 16 September 2022).
45. Gerogiannopoulos, N.G.; Brown, E.T. The critical state concept applied to rock. *Int. J. Rock Mech. Min. Sci.* **1978**, *15*, 1–10. [CrossRef]
46. Hawkes, C.D.; Bachu, S.; Haug, K.; Thompson, A.W. Analysis of in-situ stress regime in the Alberta Basin, Canada, for performance assessment of CO₂ geological sequestration sites. In Proceedings of the Fourth Annual Conference on Carbon Capture and Sequestration DOE/NETL, Alexandria, VA, USA, 2–5 May 2005; pp. 2–5.
47. Mclellan, P.J. In-Situ stress prediction and measurement by hydraulic fracturing, Wapiti, Alberta. *J. Can. Pet. Technol.* **1988**, *27*, 85–96. [CrossRef]
48. Alberta Energy Regulator. *Directive 040: Pressure and Deliverability Testing Oil and Gas Wells*; Alberta Energy Regulator: Edmonton, AB, Canada, 2020; Available online: <https://static.aer.ca/prd/documents/directives/Directive040.pdf> (accessed on 16 September 2022).
49. Bell, J.S.; Grasby, S.E. The stress regime of the Western Canadian Sedimentary Basin. *Geofluids* **2012**, *12*, 150–165. [CrossRef]
50. Schultz, R.; Wang, R.; Gu, Y.J.; Haug, K.; Atkinson, G. A seismological overview of the induced earthquakes in the Duvernay play near Fox Creek, Alberta. *J. Geophys. Res. Solid Earth* **2017**, *122*, 492–505. [CrossRef]
51. Bailey, A.; Tenthorey, E.; Ayling, B. Characterising the present-day stress regime of the Georgina Basin. *Aust. J. Earth Sci.* **2017**, *64*, 121–136. [CrossRef]
52. Brudy, M.; Zoback, M.D.; Fuchs, K.; Rummel, F.; Baumgärtner, J. Estimation of the complete stress tensor to 8 km depth in the KTB scientific drill holes: Implications for crustal strength. *J. Geophys. Res. B Solid Earth* **1997**, *102*, 18453–18475. [CrossRef]
53. van der Baan, M.; Calixto, F. Human-induced seismicity and large-scale hydrocarbon production in the USA and Canada. *Geochem. Geophys. Geosystems* **2017**, *18*, 2467–2485. [CrossRef]
54. Shen, L.W.; Schmitt, D.R.; Schultz, R. Frictional Stabilities on Induced Earthquake Fault Planes at Fox Creek, Alberta: A Pore Fluid Pressure Dilemma. *Geophys. Res. Lett.* **2019**, *46*, 8753–8762. [CrossRef]
55. Zhang, H.; Eaton, D.W.; Rodriguez, G.; Jia, S.Q. Source-mechanism analysis and stress inversion for hydraulic-fracturing-induced event sequences near fox Creek, Alberta. *Bull. Seismol. Soc. Am.* **2019**, *109*, 636–651. [CrossRef]
56. Shen, L.W.; Schmitt, D.R.; Wang, R.; Hauck, T.E. States of In Situ Stress in the Duvernay East Shale Basin and Willesden Green of Alberta, Canada: Variable In Situ Stress States Effect Fault Stability. *J. Geophys. Res. Solid Earth* **2021**, *126*, e2020JB021221. [CrossRef]
57. Ferguson, G. Deep injection of waste water in the Western Canada Sedimentary Basin. *Groundwater* **2015**, *53*, 187–194. [CrossRef]
58. Menendez, B.; Zhu, W.; Wong, T.-F. Micromechanics of brittle faulting and cataclastic flow in Berea sandstone. *J. Struct. Geol.* **1996**, *18*, 1–16. [CrossRef]
59. Austin, N.J.; Kennedy, L.A.; Logan, J.M.; Rodway, R. Textural controls on the brittle deformation of dolomite: The transition from brittle faulting to cataclastic flow. *Geol. Soc. Spec. Publ.* **2005**, *243*, 51–66. [CrossRef]
60. Imperial Oil Resources Ventures Ltd. *Application for Cold Lake Solvent Assisted SAGD Project Expansion: Attachment 2 Cold Lake Expansion Project Fracture Characterization*; Imperial Oil Resources Ventures Ltd.: Edmonton, AB, Canada, 2016; Available online: <https://open.alberta.ca/dataset/8a060768-ed57-47d4-aea3-0fb8577b646e/resource/72cc92f0-ebb9-4848-8e8d-b169ac04b0c2/download/vol1-attachment2.pdf> (accessed on 16 September 2022).
61. Hein, F.J.; Fairgrieve, B.; Dolby, G. Heavy-oil and Oil-sand Petroleum Systems in Alberta and Beyond. In *AAPG Studies in Geology*; American Association of Petroleum Geologists: Tulsa, OK, USA, 2012; pp. 207–249.
62. Dusseault, M.B.; Morgenstern, N.R. Locked sands. *Q. J. Eng. Geol.* **1979**, *12*, 117–131. [CrossRef]
63. Abdelaziz, T.S.; Martin, C.D.; Chalaturnyk, R.J. Characterization of locked sand from northeastern Alberta. *Geotech. Test. J.* **2008**, *31*, 480–489. [CrossRef]
64. Mckean, S.H.; Priest, J.A.; Eaton, D.W. A geomechanical comparison of the Duvernay and the Montney. In Proceedings of the GeoConvention, Calgary, AB, Canada, 7–11 May 2018; pp. 1–5.

65. Kim, S.; Hosseini, S.A. Study on the ratio of pore-pressure/stress changes during fluid injection and its implications for CO₂ geologic storage. *J. Pet. Sci. Eng.* **2017**, *149*, 138–150. [[CrossRef](#)]
66. Roland, E.; McGuire, J.J. Earthquake swarms on transform faults. *Geophys. J. Int.* **2009**, *178*, 1677–1690. [[CrossRef](#)]
67. Passelègue, F.X.; Aubry, J.; Nicolas, A.; Fondriest, M.; Deldicque, D.; Schubnel, A.; Di Toro, G. From fault creep to slow and fast earthquakes in carbonates. *Geology* **2019**, *47*, 744–748. [[CrossRef](#)]
68. Eyre, T.S.; Zecevic, M.; Salvage, R.O.; Eaton, D.W. A long-lived swarm of hydraulic fracturing-induced seismicity provides evidence for aseismic slip. *Bull. Seismol. Soc. Am.* **2020**, *110*, 2205–2215. [[CrossRef](#)]
69. Igonin, N.; Verdon, J.P.; Eaton, D.W. Seismic Anisotropy Reveals Stress Changes around a Fault as It Is Activated by Hydraulic Fracturing. *Seismol. Res. Lett.* **2022**, *93*, 1737–1752. [[CrossRef](#)]
70. Yu, H.; Harrington, R.M.; Kao, H.; Liu, Y.; Wang, B. Fluid-injection-induced earthquakes characterized by hybrid-frequency waveforms manifest the transition from aseismic to seismic slip. *Nat. Commun.* **2021**, *12*, 6862. [[CrossRef](#)]
71. Eyre, T.S.; Samsonov, S.; Feng, W.; Kao, H.; Eaton, D.W. InSAR data reveal that the largest hydraulic fracturing-induced earthquake in Canada, to date, is a slow-slip event. *Sci. Rep.* **2022**, *12*, 2043. [[CrossRef](#)]
72. Riazi, N.; Eaton, D.W.; Aklilu, A.; Poulin, A. Application of focal-time analysis for improved induced seismicity depth control: A case study from the Montney Formation, British Columbia, Canada. *Geophysics* **2020**, *85*, KS185–KS196. [[CrossRef](#)]
73. Li, T.; Gu, J.; Wang, R.; Yusifbayov, J.; Canales, M.; Shipman, T. Earthquakes Induced by Wastewater Disposal near Musreau Lake, Alberta, 2018–2020. *Seismol. Res. Lett.* **2022**, *93*, 727–738. [[CrossRef](#)]
74. Schultz, R.; Mei, S.; Pană, D.; Stern, V.; Gu, Y.J.; Kim, A.; Eato, D. The Cardston earthquake swarm and hydraulic fracturing of the Exshaw formation (Alberta Bakken play). *Bull. Seismol. Soc. Am.* **2015**, *105*, 2871–2884. [[CrossRef](#)]
75. Schultz, R.; Stern, V.; Gu, Y.J. An investigation of seismicity clustered near the Cordel Field, west central Alberta, and its relation to a nearby disposal well. *J. Geophys. Res. Solid Earth* **2014**, *119*, 3410–3423. [[CrossRef](#)]
76. Salvage, R.O.; Eaton, D.W. The Influence of a Transitional Stress Regime on the Source Characteristics of Induced Seismicity and Fault Activation: Evidence from the 30 November 2018 Fort St. John ML 4. 5 Induced Earthquake Sequence. *Bull. Seismol. Soc. Am.* **2022**, *112*, 1336–1355. [[CrossRef](#)]
77. Fjaer, E.; Holt, R.M.; Horsrud, P.; Raaen, A.M.; Risnes, R. *Petroleum Related Rock Mechanics*, 2nd ed.; Elsevier: Amsterdam, The Netherlands, 2008; Volume 9.
78. Roche, V.; Van Der Baan, M. The role of lithological layering and pore pressure on fluid-induced microseismicity. *J. Geophys. Res. Solid Earth* **2015**, *120*, 923–943. [[CrossRef](#)]
79. Bhattacharya, P.; Viesca, R.C. Fluid-induced aseismic fault slip outpaces pore-fluid migration. *Science* **2019**, *364*, 464–468. [[CrossRef](#)]
80. Cappa, F.; Guglielmi, Y.; Nussbaum, C.; Birkholzer, J. On the Relationship between Fault Permeability Increases, Induced Stress Perturbation, and the Growth of Aseismic Slip during Fluid Injection. *Geophys. Res. Lett.* **2018**, *45*, 11012–11020. [[CrossRef](#)]
81. Hui, G.; Chen, S.; Chen, Z.; Gu, F. Integration of geophysics, geomechanics and hydrodynamics to characterize induced seismicity triggered by hydraulic fracturing in the Duvernay reservoir near Fox Creek, Alberta. In Proceedings of the 53rd U.S. Rock Mechanics/Geomechanics Symposium, New York, NY, USA, 23–26 June 2019; pp. 1–6.
82. Han, H.; Yin, S.; Chen, Z.; Dussault, M.B. Estimate of in-situ stress and geomechanical parameters for Duvernay Formation based on borehole deformation data. *J. Pet. Sci. Eng.* **2021**, *196*, 107994. [[CrossRef](#)]
83. Shen, L.W.; Schmitt, D.R.; Haug, K. Quantitative constraints to the complete state of stress from the combined borehole and focal mechanism inversions: Fox Creek, Alberta. *Tectonophysics* **2019**, *764*, 110–123. [[CrossRef](#)]
84. Carmen, C.; Talinga, D.A. Overburden characterization with formation pore pressure and anisotropic stress field estimation in the Athabasca Basin, Canada. *Interpretation* **2019**, *7*, 761–771. [[CrossRef](#)]
85. Kry, P.R.; Gronseth, J.M. In-Situ Stresses and Hydraulic Fracturing in the Deep Basin. *J. Can. Pet. Technol.* **1983**, *22*, 31–35. [[CrossRef](#)]
86. Bell, J.S.; Bachu, S. In Situ stress magnitude and orientation estimates for Cretaceous coal-bearing strata beneath the plains area of central and southern Alberta. *Bull. Can. Pet. Geol.* **2003**, *51*, 1–28. [[CrossRef](#)]
87. Bachu, S.; Brydie, J.; Hauck, T.; Lakeman, B.; Palombi, D.; Stoakes, F.; Wendte, J.; Lawton, D.; Darvish, M.P.; Hawkes, C.; et al. The Heartland Area Redwater CO₂ storage project (HARP): Results of Phase I site characterization. *Energy Procedia* **2011**, *4*, 4559–4566. [[CrossRef](#)]
88. Keneti, S.A.R.; Wong, R.C.K. Investigation of anisotropic behavior of Montney shale under indirect tensile strength test. In Proceedings of the Canadian Unconventional Resources and International Petroleum Conference, Calgary, AB, Canada, 19–21 October 2010; Society of Petroleum Engineers. OnePetro: Richardson, TX, USA, 2010; Volume 4, pp. 2583–2591. [[CrossRef](#)]
89. Contreras, O.; Hareland, G.; Aguilera, R. Pore pressure modelling and stress-faulting-regime determination of the Montney shale in the Western Canada Sedimentary Basin. *J. Can. Pet. Technol.* **2013**, *52*, 349–359. [[CrossRef](#)]
90. Jimenez, B.L.; Yu, G.; Aguilera, R.; Settari, A. Calibration of well logs with mini-frac data for estimating the minimum horizontal stress in the tight-gas Monteith formation of the Western Canada Sedimentary Basin: A case study. *SPE Prod. Oper.* **2015**, *30*, 110–120. [[CrossRef](#)]
91. Cui, A.; Glover, K.; Wust, R. Elastic and plastic mechanical properties of liquid-rich unconventional shales and their implications for hydraulic fracturing and proppant embedment: A case study of the Nordegg Member in Alberta, Canada. In Proceedings of the 48th U.S. Rock Mechanics/Geomechanics Symposium, Minneapolis, MN, USA, 1–4 June 2014; Volume 2, pp. 822–833.

92. Roney, D.; Quirk, D.; Ziarani, A.S.; Burke, L. Integration of microseismic data, tracer information, and fracture modeling into the development of fractured horizontal wells in the Slave Point Formation. *Soc. Pet. Eng. SPE Can. Unconv. Resour. Conf.* **2014**, *1*, 480–497. [[CrossRef](#)]
93. Statoil Hydro. *Application for Approval of Kai Kos Dehseh Project—SIR Round 3*; Statoil Hydro: Edmonton, AB, Canada, 2009; Available online: <https://open.alberta.ca/dataset/7017ad9b-f8da-4ca2-b2be-2f6a073d58f2/resource/02292fca-2bec-4823-ad2d-00104bd09c99/download/kkd-sir-round-3.pdf> (accessed on 16 September 2022).
94. Alberta Innovates. *Technology Futures Appendix D: Geomechanical Analysis of the Effects of CO₂ Injection in the Leduc (D3-A) and Nisku (D-2) Reservoirs in the Clive Field*; Alberta Innovates: Edmonton, AB, Canada, 2019; Available online: <https://open.alberta.ca/dataset/90f61413-0ef1-45a4-9e1c-6bff7c23fd7e/resource/17d13263-5527-4f56-bed9-112fe1353241/download/energy-actl-enhance-energy-clive-leduc-field-mmvp-plan-appendices-2019-07.pdf> (accessed on 16 September 2022).
95. Canadian Discovery Ltd. *Characterization of the Belloy and Debolt Water Disposal Zones in the Montney Play Fairway, Northeastern BC*; Canadian Discovery Ltd.: Victoria, BC, Canada, 2015; Available online: <https://www.geosciencebc.com/geoscience-bc-releases-study-results-identifying-water-disposal-zones-in-northeast-bc/> (accessed on 16 September 2022).
96. Goodarzi, S.; Settari, A.; Ghaderi, S.M.; Hawkes, C.; Leonenko, Y.; Leonenko, Y. The effect of site characterization data on injection capacity and cap rock integrity modeling during carbon dioxide storage in the Nisku saline aquifer at the Wabamun Lake area, Canada. *Environ. Geosci.* **2020**, *27*, 49–65. [[CrossRef](#)]
97. Costin, S.; Smith, R.; Yuan, Y.; Andjelkovic, D.; Garcia Rosas, G. In-Situ Stresses in Colorado Group, AB, Calculated from Open-Hole Mini-Fracs and FMI Logs. In Proceedings of the SPE Annual Technical Conference and Exhibition, Calgary, AB, Canada, 30 September–2 October 2019; SPE-196037-MS. SPE: Calgary, AB, Canada, 2019; pp. 1–25.
98. Morin, M.L. *Natural and Drilling Induced Fractures in the Grosmont Formation, Alberta: Implications for the State of Stress*. Master's Thesis, University of Alberta, Edmonton, AB, Canada, 2017.
99. Imperial Oil Resources Ventures Ltd. *Application for Approval of the Aspen Project: Volume 1*; Imperial Oil Resources Ventures Ltd.: Edmonton, AB, Canada, 2013; Available online: <https://static1.squarespace.com/static/52abb9b9e4b0cb06a591754d/t/5dd7383c761fa94d312c8ccb/1574385753225/xVol1-Project-Description+%28Geology%29.pdf> (accessed on 16 September 2022).
100. Prosper Petroleum Ltd. *Application for Approval of the Rigel Oil Sands Project*; Prosper Petroleum Ltd.: Edmonton, AB, Canada, 2013; Available online: <https://prosperpetroleum.com/wp-content/uploads/2015/06/Rigel-Oil-Sands-Project-ApplicationB.compressed.pdf> (accessed on 16 September 2022).
101. Liu, J.G.; Xu, B.; Sun, L.; Li, B.; Wei, G.J. In Situ stress field in the Athabasca oil sands deposits: Field measurement, stress-field modeling, and engineering implications. *J. Pet. Sci. Eng.* **2022**, *215*, 110671. [[CrossRef](#)]